



This is the accepted manuscript made available via CHORUS. The article has been published as:

Discerning element and site-specific fluctuations of the  
charge-orbital order in  $\text{FeMn}_3\text{O}_4$  below the Verwey transition

Nelson Hua, Jianheng Li, Stjepan B. Hrkac, Andi Barbour, Wen Hu, Claudio Mazzoli, Stuart Wilkins, Roopali Kukreja, Eric E. Fullerton, and Oleg G. Shpyrko

Phys. Rev. Materials **7**, 014413 — Published 31 January 2023

DOI: [10.1103/PhysRevMaterials.7.014413](https://doi.org/10.1103/PhysRevMaterials.7.014413)

# Discerning Element and Site-Specific Fluctuations of the Charge-Orbital Order in $\text{Fe}_3\text{O}_4$ below the Verwey Transition

Nelson Hua<sup>1,2</sup>, Jianheng Li<sup>3</sup>, Stjepan B. Hrkac<sup>1</sup>, Andi Barbour<sup>4</sup>, Wen Hu<sup>4</sup>, Claudio Mazzoli<sup>4</sup>, Stuart Wilkins<sup>4</sup>, Roopali Kukreja<sup>3,\*</sup>, Eric E. Fullerton<sup>1,2</sup>, Oleg G. Shpyrko<sup>1,2,\*\*</sup>

<sup>1</sup>Department of Physics, University of California, San Diego, La Jolla, California, 92093, USA

<sup>2</sup>Center for Memory and Recording Research, University of California, San Diego, La Jolla, California, 92093, USA

<sup>3</sup>Department of Materials Science Engineering, University of California, Davis, Davis, California, 95616, USA

<sup>4</sup>National Synchrotron Light Source II, Brookhaven National Laboratory, Upton, New York 11973, USA

*Despite countless experimental probes into magnetite's electronic structure across the Verwey transition  $\text{Fe}_3\text{O}_4$ , the exact origin of this archetypical metal-insulator transition remains a puzzle. Advanced x-ray diffraction techniques have mostly resolved the monoclinic structure of the insulating phase, including interatomic bond lengths, but the complexity of the charge-orbitally ordered state is difficult to disentangle. We combined resonant elastic x-ray scattering and x-ray photon correlation spectroscopy to probe charge-orbital fluctuations in the insulating state of magnetite. By accessing the Bragg forbidden  $(00\frac{1}{2})_c$  peak at the O K edge, we complement our previous study on the Fe  $L_3$ -edge (R. Kukreja et al., Phys. Rev. Lett. 2018) to reveal the dynamics of the Fe 3d and O 2p orbital domains. Our new results reveal a decoupling of the orbital correlation lengths between the O 2p states and site-specific Fe 3d states, and we further show charge-orbital domain fluctuations in the Fe  $t_{2g}$  orbital sites of trimeron chains. These results also demonstrate an experimental method capable of distinguishing electronic dynamics between the oxygen ligands and the transition metal that underpins emergent behaviors in complex oxides.*

## Introduction

Macroscopic phenomena in transition-metal oxides such as superconductivity, colossal magnetoresistance, and metal-insulator transitions are manifestations of the correlations between the electronic and lattice structures at the atomic scale [1–3]. Resolving competing order parameters originating from the electron spin, charge, and orbital states as well as mesoscale effects such as domain wall evolution is key to understanding how to tailor these materials for electronic applications. One approach to resolving various structural and electronic order parameters is with elastic x-ray scattering techniques, which have been frequently used to study the role of the transition metal [4–7]. However, the role of the oxygen ligands is often neglected given that the accessibility of oxygen in scattering is often difficult or impossible to reach, and many techniques such as x-ray magnetic circular and linear dichroism only make sense about the transition metal resonant edges. In this study, we use a coherent x-ray scattering technique known as X-ray Photon Correlation Spectroscopy (XPCS) at the O *K*-edge resonance to study possible dynamic behavior of oxygen in Fe<sub>3</sub>O<sub>4</sub> that would otherwise be hidden from standard x-ray diffraction techniques.

In magnetite (Fe<sub>3</sub>O<sub>4</sub>), the mechanism behind its metal-insulator transition, famously known as the Verwey transition, continues to confound physicists. In the high-temperature metallic state, magnetite has a cubic inverse spinel structure consisting of two sublattices. The *A* sites are characterized by O<sup>2-</sup> and Fe<sup>3+</sup> ions that are tetrahedrally coordinated while *B* sites are octahedrally coordinated consisting of O<sup>2-</sup> ions and [Fe<sup>2+</sup>, Fe<sup>3+</sup>] ions in equal proportion [8,9]. The iron atoms of the *A* and *B* sites are also antiferromagnetically coupled through hybridization with the oxygen 2p orbitals. When magnetite is cooled below the transition temperature  $T_v \sim 120$  K, a structural phase transition occurs where the cubic structure ( $a=b=c=8.387$  Å) distorts to a monoclinic one ( $a=b=11.88$  Å,  $c = 16.775$  Å and  $\beta = 90.236^\circ$ ) and is simultaneously accompanied by a drop in electrical conductivity by two to three orders of magnitude [10,11]. Verwey postulated that this insulating state arises from the freezing of a *B*-site conduction electron into a charge-ordered state of alternating

$\text{Fe}^{2+}$  and  $\text{Fe}^{3+}$  on the octahedral sublattice [11]. Although experiments have since disproven Verwey's original theory, a significantly more complex charge and orbitally-ordered insulating state is seen below the transition temperature.

In the monoclinic phase, cooperative Jahn-Teller (JT) distortions shorten interatomic bond lengths of *B*-site Fe cations into linear three-site chains known as trimerons, the proposed order parameter describing the charge-orbitally ordered insulating state [12,13]. In particular, a trimeron consists of *B*-site iron atoms that are charge ordered in  $\text{Fe}^{3+}$ -  $\text{Fe}^{2+}$ -  $\text{Fe}^{3+}$  chains where the extra electron occupation of the degenerate Fe- $t_{2g}$  orbitals give rise to an additional orbitally ordered structure as seen in Fig. 1a. In transition-metal oxides, Kugel and Khomskii have shown that orbital ordering arises from either JT coupling of electrons to the lattice or hopping of transition metal electrons into specific orbital states [14–16]. In the case of magnetite, the charge-orbital order manifests as a Bragg forbidden  $(00\frac{1}{2})_c$  (the subscript denotes the cubic notation) peak that is accessible only at iron and oxygen resonant energies [17–19]. In other words, the charge-orbital anisotropy leads to a non-zero scattering factor at resonant energies [20]. The stability of this charge-orbital structure can be determined by changes in the orbital occupations at both the iron and oxygen sites [21]. Previously, we accessed the  $(00\frac{1}{2})_c$  peak in scattering geometry at the Fe  $L_3$ -edge to probe the Fe 3d orbital occupancies via excitations from core to unoccupied valence states at the Fe  $2p_{3/2} \rightarrow 3d$  transitions [18]. The Fe  $L_3$ -edge signal directly probes the *B*-site  $\text{Fe}^{2+}$   $t_{2g}$  orbital structure, and our results showed dynamic orbital domain fluctuations in the low-temperature state. However, the results at the Fe  $L_3$ -edge alone are not sufficient to pinpoint the origin of those fluctuations. We combined resonant elastic x-ray scattering (REXS) and XPCS at the O *K*-edge to further investigate the origin of these orbital fluctuations, whether it is due to structural domain reorientations or purely electronic in nature. The resonant O *K*-edge  $(00\frac{1}{2})_c$  peak in scattering geometry directly probes the O 2p orbital occupancies via excitations from core to unoccupied valence states at the O  $1s \rightarrow 2p$  transitions. Previous studies using resonant elastic x-ray scattering and local density approximation (LDA + U) calculations show this peak arising from orbitally-

ordered O 2p states. Since the O 2p states are also hybridized to the Fe 3d orbitals present on both the octahedral and tetrahedral sites as seen in Figs. 1a and 1b [18,19,22–24], we can also indirectly probe the Fe 3d state. Previous simulations have shown this signal to be mostly sensitive to the hybridization to the *B*-site Fe<sup>3+</sup> ions. Our studies show a lack of electronic fluctuations at the O *K*-edge, indicating an extremely stable oxygen 2p orbital network in the low-temperature monoclinic phase where there is an absence of ligand-to-metal charge transfer dynamics in equilibrium. This implies that the thermally active fluctuations previously observed in the Fe *t*<sub>2g</sub> orbital domains is due to the delocalization of the minority spin electron between adjacent *B*-site Fe cations within trimeron chains, as postulated by Senn *et. al* [12]. Our XPCS studies at both the Fe *L*<sub>3</sub>-edge and the O *K*-edge are now able to experimentally confirm this scenario.

### Experiment and Results

The resonant XPCS experiment was conducted at the Coherent Soft X-ray (CSX) beamline at the National Synchrotron Light Source II (NSLS-II). A schematic of the experimental scattering geometry is shown in Fig. 2 where a coherent x-ray beam is tuned to the Fe *L*<sub>3</sub>-edge (705.7 eV) and O *K*-edge (527.2 eV) resonant energies to probe the  $(00\frac{1}{2})_c$  peak where the slight offset from literature values is due to the calibration at the beamline. The resonant energy at the Fe *L*<sub>3</sub>-edge corresponds to the maximum scattered intensity at the  $(00\frac{1}{2})_c$  Bragg condition, which was previously shown to be mainly due to the B-site Fe<sup>2+</sup> cations from the decomposition of the x-ray absorption spectroscopy (XAS) spectrum [18,22,25]. The O *K*-edge resonant energy was also optimized to the maximum scattering intensity at the  $(00\frac{1}{2})_c$  Bragg condition corresponding to the pre-edge of the O *K*-edge XAS profile [19]. The (001) lattice peak is also only accessible in the monoclinic phase based on the crystal symmetry of the low-temperature state [17]. Therefore, we also monitored the (001) lattice peak profile off resonance at 800 eV to independently follow the correlation length of the structural order. A CCD detector with 30 μm x 30 μm pixel size located 34 cm from the sample was used to record the measurements, and an example of the detector image for the  $(00\frac{1}{2})_c$  peak at the O *K*-edge resonance is shown in Fig. 2. The

degree of contrast can be visualized from a line cut through the central speckle pattern as shown in Fig. 3a. A Gaussian function was used to fit the peak where the full-width-at-half-maximum (FWHM) in reciprocal space,  $\Delta Q$ , is used to define the correlation length  $\lambda = 1/\Delta Q$ . Superimposed in Fig. 3a is the (001) lattice peak at 800 eV that shows the correlation length of the lattice structure is approximately ten times greater than the charge-orbital correlation length, indicating the oxygen 2p orbital domains are not defined by structural domain boundaries. The  $(00\frac{1}{2})_c$  peak at the O *K*-edge resonance was measured between 25 K to 109 K and its correlation length and integrated peak intensity as a function of temperature are shown in Fig. 3b. The correlation lengths of the  $(00\frac{1}{2})_c$  peak at the O *K*-edge and Fe *L*<sub>3</sub>-edge well below the Verwey transition temperature are approximately 13 nm and 16 nm respectively, which is consistent with literature data [18,26,27].

The speckle pattern overlaid on the  $(00\frac{1}{2})_c$  peak is the fundamental attribute in the XPCS technique that allows us to measure dynamics of the system. When a coherent beam interacts with the nanoscale heterogeneities, in this case charge-orbital domains, the interference between the coherent beam and the nanoscale heterogeneities creates the speckle pattern seen within the  $(00\frac{1}{2})_c$  peak. Since we have a stable coherent beam, any fluctuations of the charge-orbital domains manifest as spatial and temporal intensity changes in the speckle pattern. Therefore, by correlating the intensity of successive speckle patterns, it is possible to resolve the dynamic timescale of the system from how fast or slow the speckle pattern decorrelates in time. This can be quantified by the two-time intensity-intensity autocorrelation function given in Eq. 1 where the intensity of the  $(00\frac{1}{2})_c$  peak is correlated pixel-by-pixel with itself at different times,  $t_1$  and  $t_2$ , during the entire scan. The normalized correlation plots for the Fe *L*<sub>3</sub>-edge and O *K*-edge at 85 K, 90 K, and 100 K are shown in Fig. 4, but the first 30-45 minutes of each scan can be ignored due to instability as the sample equilibrated. The two-time correlation plots for all temperature measurements between 25 K and 109 K can be found in the Supplemental Material section [28].

$$g_2(q, t_1, t_2) = \frac{\langle I(q, t_1)I(q, t_2) \rangle}{\langle I(q, t_1) \rangle \langle I(q, t_2) \rangle} \quad (1)$$

From the correlation plots, we see the signal at the Fe  $L_3$ -edge is continuously dynamic throughout the scan while a static signal is seen at the O  $K$ -edge. After normalizing to the average intensity of the speckle pattern, the  $t_1 = t_2$  line is the fully correlated reference value while lines orthogonal to  $t_1 = t_2$  show increasing delay time between speckle patterns. In Fig. 4, the region where the sample is stable is marked by the dotted black lines, and for the O  $K$ -edge signal, the correlation value is approximately the same as the  $t_1 = t_2$  value at all points, indicative of a static signal. On the other hand, the correlation value drops away from the  $t_1 = t_2$  line for the Fe  $L_3$ -edge, showing the speckle pattern is changing in time. We previously showed the dynamics speed up and follow an Arrhenius trend up to 90 K, but slow down until the insulator-to-metal transition temperature at  $T = 116$  K [26]. An increasing amount of metallic domains above 90 K spatially reduce the trimeron network, and thus the available hopping sites for the electron. With new results from the O  $K$ -edge, we can further conclude that while metallic domains govern the change of characteristic dynamic timescales at the B-site Fe  $t_{2g}$  states, at a given temperature, the configuration of metallic domains remains static. Both the O  $K$ -edge and Fe  $L_3$ -edge resonant signals are only sensitive to the insulating phase which can be seen from the drop in total intensity as metallic domains begin to nucleate approaching the metal-insulator transition temperature. If enough thermal energy exists to drive structural fluctuations between metallic and insulating phases at each temperature, that would manifest as a dynamic speckle pattern at both the O  $K$ -edge and Fe  $L_3$ -edge. The static signal at the O  $K$ -edge indicates an absence of structural fluctuations between metallic and insulating domains and therefore cannot be the source of the dynamics observed at the Fe  $L_3$ -edge.

### Discussion

Ruling out any structural fluctuations, the origin of the dynamic speckle pattern at the Fe  $L_3$ -edge and the static speckle pattern at the O  $K$ -edge must be electronic in nature.

The speckle pattern at the Fe  $L_3$ -edge is a fingerprint of the orbital-specific electron occupancies, i.e. the unique configuration of  $\text{Fe}^{2+}$  and  $\text{Fe}^{3+}$  occupying the  $t_{2g}$  orbitals, and any rearrangements to this configuration would alter the speckle pattern. Therefore, the dynamic speckle pattern at the Fe  $L_3$ -edge indicates a rearrangement of the  $\text{Fe}^{2+}$  and  $\text{Fe}^{3+}$  ions within trimeron chains that can only be attributed to thermally-driven charge hopping of the conduction electrons. While the charge hopping mechanism itself is ultrafast and beyond our experimental capabilities, the large activation energy and long timescales observed at the Fe  $L_3$ -edge indicate that the rate of the charge hopping is infrequent where the overall trimeron network evolves on the order of minutes [26]. Based on well-established theory on orbital ordering in transition-metal oxides and recent studies of the trimeron network [21,26,29], the strength of orbital hybridizations, and consequently the potential for charge dynamics, depends on the degree of orbital overlap between neighboring sites. In the case of magnetite, the interatomic distances of Fe cations are shortened within trimeron chains, creating an even stronger orbital overlap that allows for charge dynamics amongst the Fe cations [12]. Density functional theory and optical magnetic circular dichroism measurements show three dominant pathways for charge dynamics in magnetite [30, 31], including direct hopping between neighboring Fe-Fe sites along the trimeron chains, depicted in Fig. 1a, and the oxygen-mediated charge transfer via superexchange and double exchange interactions shown in Fig. 1b. There is also a ligand-to-metal  $p - d$  charge transfer tied to the O 2p to  $\text{Fe}^{2+}$  3d pathway [30] that we can directly detect in our measurements.

The speckle pattern at the O  $K$ -edge is a manifestation of the configuration of both the occupied and unoccupied 2p orbitals that are also hybridized to the  $B$ -site Fe  $t_{2g}$  orbitals, giving rise to the aforementioned charge transfer pathways. While superexchange and double exchange interactions will not alter the final state of the oxygen orbital occupations, any direct ligand-to-metal charge dynamics would change the configuration of the oxygen 2p orbital network, manifesting as a fluctuating speckle pattern. Our static signal at the O  $K$ -edge demonstrates an absence of this pathway in equilibrium, suggesting the charge dynamics in the insulating state of magnetite is due purely to the minority spin electron



along the trimeron chains. Finally, the orbital correlation lengths of the *B*-site Fe  $t_{2g}$  orbitals (16 nm) and O 2p orbitals (13 nm) at  $T = 27$  K are on the same order of magnitude. However, this disparity is significant as it corresponds to a FWHM difference of approximately  $\sim 100$  pixels in our experimental conditions, well beyond the error of margin. Even though the intricately linked Fe  $t_{2g}$  and O 2p orbitals give rise to the resonant  $(00\frac{1}{2})_c$  peak, the difference in orbital correlation lengths suggests there is still an unknown mechanism that leads to this spatial decoupling. This is also supported by the anomalous uptick of the correlation length near the transition temperature seen in Fig. 3b and a similar anomalous uptick in the peak intensity in seen in [22], both of which are seen at the O *K*-edge but not at the Fe  $L_{3-}$  edge.

### Conclusion

We have shown an experimental approach that uses XPCS at resonant elastic geometry to directly probe the site- and element- specific charge-orbital dynamics in magnetite by exploiting a Bragg-forbidden, orbitally-ordered peak. Our results, contrary to Verwey's hypothesis that the conduction electron freezes in the insulating state, show there is still sufficient thermal energy in the system to drive these electrons to hop along trimeron chains. The extremely stable configuration of the oxygen 2p orbital network further suggests that only the minority spin electron of the Fe cations within trimeron chains play a role in the Verwey transition [32,33]. Finally, magnetite belongs to a class of transition-metal oxides where the interaction of the transition-metal 3d electrons with the field of  $O^{2-}$  ligands is responsible for many fascinating nanoscale effects that give rise to various classes of electronically ordered materials [14,24,29,34]. In this study, we specifically tuned to the O *K*-edge resonant energy and the Fe  $L_{3-}$  edge resonant energy corresponding to the O 2p and octahedral  $t_{2g}$  orbitals, respectively, but further XPCS measurements with varying polarizations at specific points in the Fe  $L_{2,3}$ -edge spectrum can reveal distinct dynamic timescales from the  $e_g$  orbitals or *A*-site Fe 3d states. With new generation coherent x-ray sources, we can employ the same experimental technique to reveal unseen dynamical trends in other materials with strong electron correlations such as nickelates and

cuprates. For example, the charge order structure of high temperature cuprate superconductors has long been attributed to the strong hybridization between the Cu 3d and O 2p orbitals, but recent studies revealed spatially localized charge excitations associated with O sites in  $\text{La}_{2-x}\text{Ce}_x\text{CuO}_4$  that seem to defy the strong hybridization between Cu and O [35]. In LBCO cuprates, resonant XPCS measurements revealed a stable charge density wave order detected at the Cu  $L_3$ -edge, but this study lacked measurements at the O  $K$ -edge [36,37]. Our XPCS study demonstrates an effective method that exploits the transition metal  $L$  edges in tandem with the oxygen  $K$  edge to pinpoint the origin of emergent behaviors.

**Acknowledgements:** The fabrication of samples at UCSD was supported by the AFOSR grant #FA9550-16-1-0026 and NSF Award DMR-1411335. The coherent x-ray scattering experiment was supported by U.S. Department of Energy, Office of Science, Office of Basic Energy Sciences, under Contract No. DE – SC0001805 (coherent x-ray scattering N.H. and O.G.S.) J.L. and R.K. were supported by a grant from the National Science Foundation (DMR-1902652). This research used resources from the 23-ID-1 Coherent Soft X-Ray Scattering (CSX) beamline of the National Synchrotron Light Source II, a U.S. Department of Energy (DOE) Office of Science User Facility operated for the DOE Office of Science by Brookhaven National Laboratory under Contract No. DE-SC0012704.

Corresponding authors: \* rkukreja@ucdavis.edu , \*\*oshpyrko@ucsd.edu

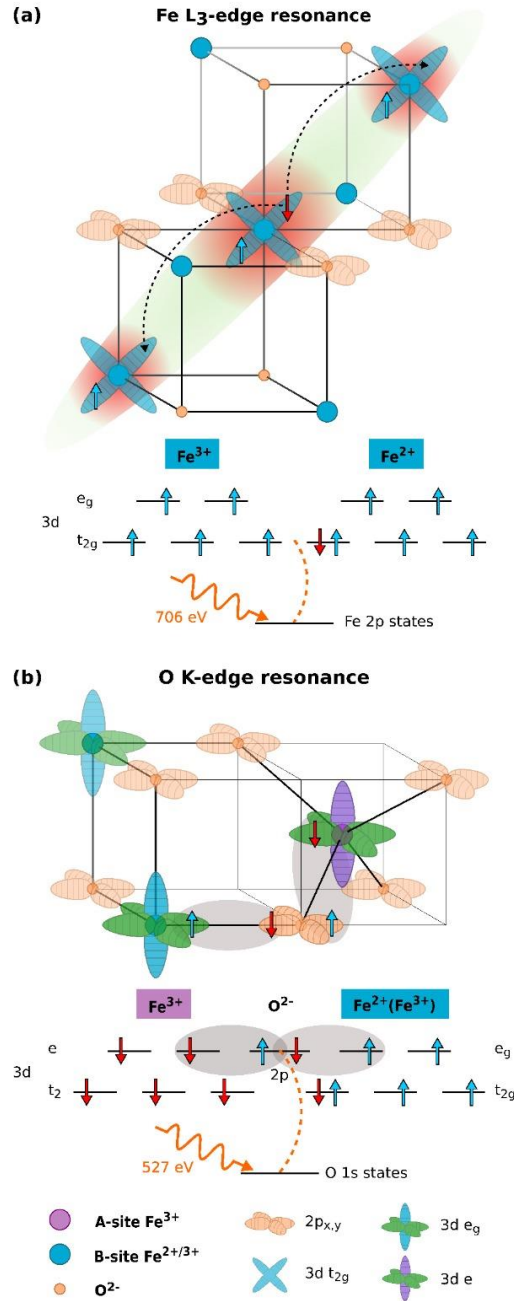


**Figure 1:** (a) Fe  $L_3$ -edge resonance ( $2p \rightarrow 3d$  states) probes the orbital occupancy of the  $t_{2g}$  electrons of specifically the B-site Fe<sup>2+</sup> cations. Since the orbital order is not linked to lattice dynamics, the signal originates from delocalization of the minority spin electron within corner sharing trimeron chains. The schematic shows one delocalization pathway where the extra electron in the central Fe<sup>2+</sup> can hop directly to neighboring Fe<sup>3+</sup>  $t_{2g}$  sites along the trimeron. (b) The gray highlighted region shows examples of how the oxygen 2p

orbitals are hybridized to the *A* and *B* iron sites, allowing for charge delocalization via superexchange and double exchange interactions.

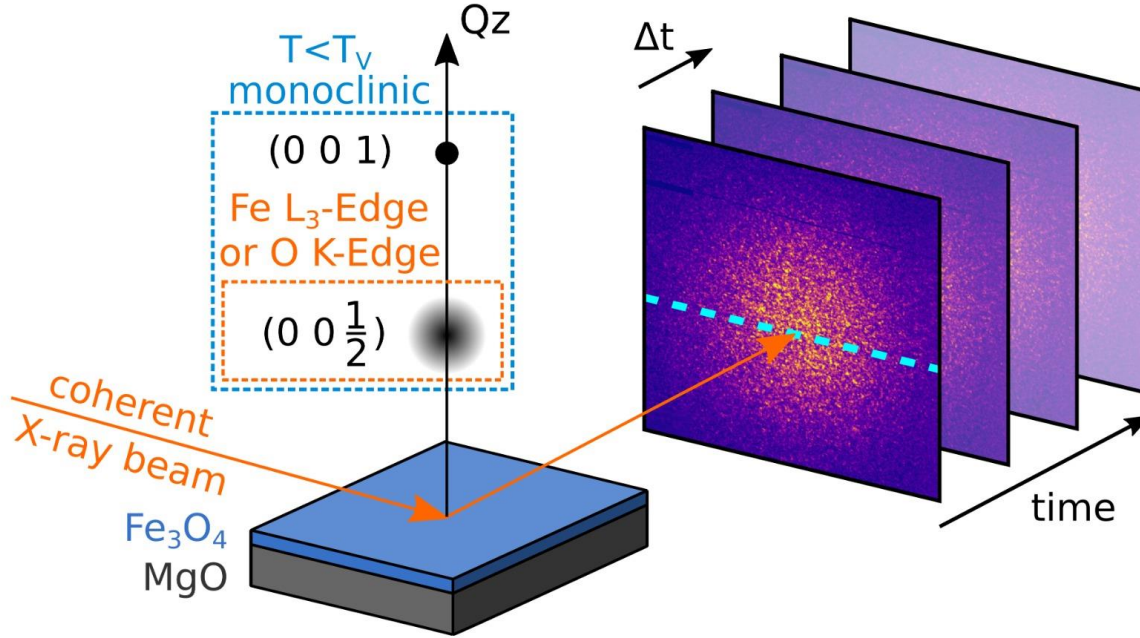


**Figure 2:** Experimental setup of the XPCS experiment where coherent soft x-rays are tuned to the Fe  $L_3$ -edge (705.7 eV) and the O  $K$ -edge (527.2 eV) to access the  $(00\frac{1}{2})_c$  peak that only exists in the low-temperature monoclinic phase at resonance. Shown is a CCD detector image of the  $(00\frac{1}{2})_c$  peak at the O  $K$ -edge resonant energy at 27 K. The  $(001)$  lattice peak is also a forbidden peak that can be accessed in the low-temperature state, though not necessarily at resonance. A CCD records the speckle pattern of the  $(00\frac{1}{2})_c$  peak at the O  $K$ -edge resonance with a delay time of  $\Delta t$  between each image.

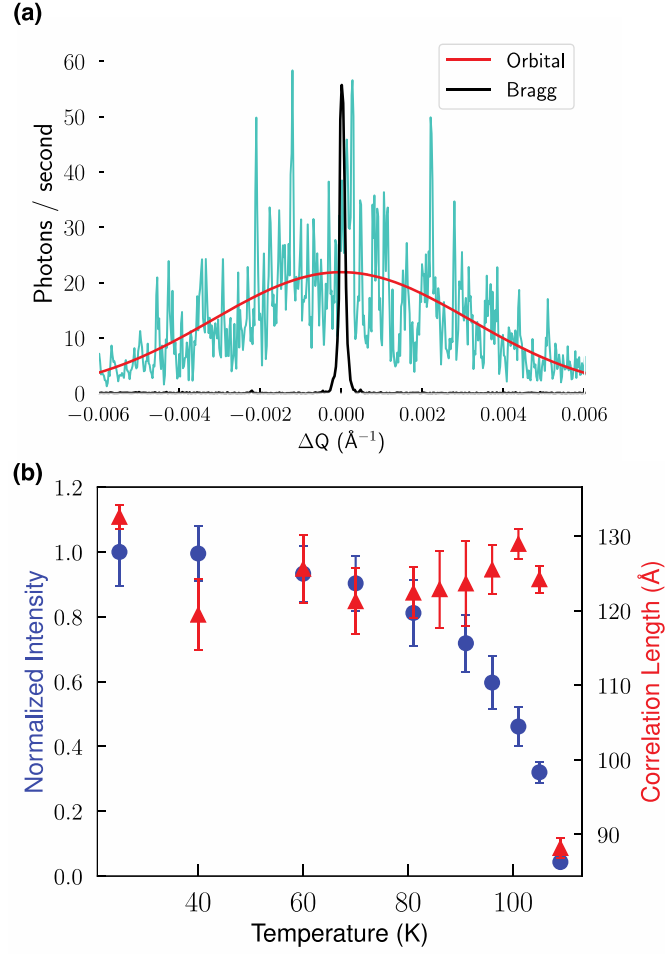


**Figure 3:** (a) A line cut through the speckle pattern in Fig. 2 that shows the degree of contrast of the signal. A Gaussian function is fitted to the  $(00\frac{1}{2})_c$  orbitally-ordered peak, and the  $(001)$  lattice reflection is superimposed to show the difference in the orbital and structural correlation lengths. (b) The normalized integrated intensity of the  $(00\frac{1}{2})_c$  peak per second at the O  $K$ -edge as a function of temperature is plotted along with the correlation length defined by  $1/\Delta Q$ , where  $\Delta Q$  is the FWHM of the Gaussian fit to the peak as seen in (a).

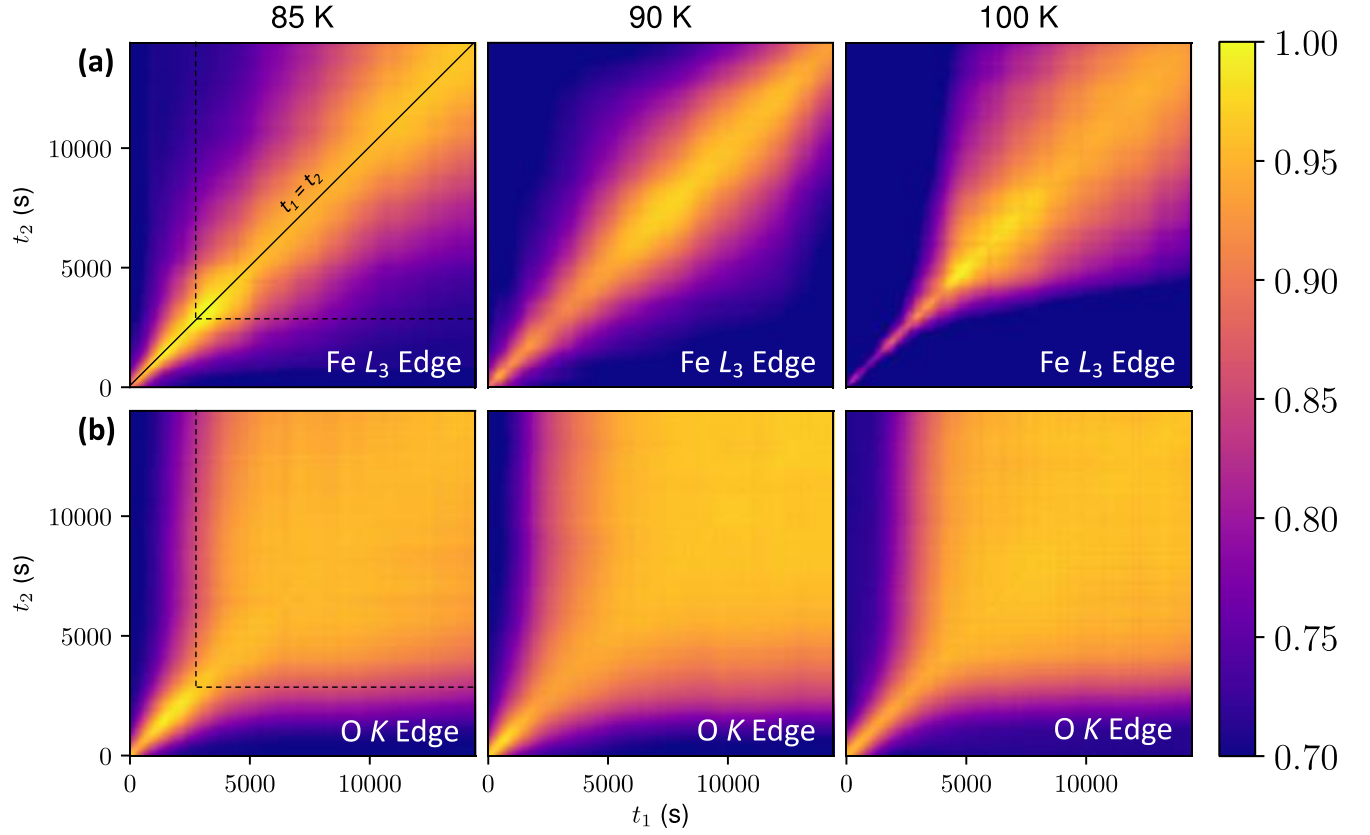


**Figure 4:** Normalized two-time intensity-intensity autocorrelation functions defined by Eq. 1 for the (a) Fe  $L_3$ -edge and the (b) O  $K$ -edge at 85 K, 90 K, and 100 K. A 1s exposure time was used for each scan that lasted 4 hours. The first 30-45 minutes of each scan is attributed to sample instability from temperature equilibration -- the approximate stable region of the scan is marked by the dotted black line. The  $(00\frac{1}{2})_c$  signal at the Fe  $L_3$ -edge that is sensitive to the Fe  $t_{2g}$  orbital structure is clearly dynamic while the O  $K$ -edge signal that is sensitive to the O  $2p$  orbital structure remains static.

## References

- [1] M. Imada, A. Fujimori, and Y. Tokura, *Rev. Mod. Phys.* **70**, 1039 (1998).
- [2] E. Dagotto, *Science* **309**, 257 (2005).
- [3] Y. Yanase, T. Jujo, T. Nomura, H. Ikeda, T. Hotta, and K. Yamada, *Phys. Rep.* **87**, (1-4) (2003).
- [4] G. Subías, J. Garcia, J. Blasco, J. Herrero-Martin, and M.C. Sánchez, *J. Phys.: Conf. Ser.* **190**, 012085 (2009).
- [5] J.J. Turner, K.J. Thomas, J.P. Hill, M.A. Pflaffer, K. Chesnel, Y. Tomioka, Y. Tokura, and S.D. Kevan, *New J. Phys.* **10**, 053023 (2008).
- [6] Y.D. Chuang, W.S. Lee, Y.F. Kung, A.P. Sorini, B. Moritz, R.G. Moore, L. Patthey, M. Trigo. D.H. Lu, P.S Kirchmann *et. al.*, *Phys. Rev. Lett.* **110**, 127404 (2013).
- [7] S.L. Zhang, A. Bauer, H. Berger, C. Pfleiderer, G. van der Laan, and T. Hesjedal, *Phys. Rev. B* **93**, 214420 (2016).
- [8] E. J. Verwey, P. W. Haayman, and F. C. Romeijn, *J. Chem. Phys.* **15**, 4 (1947).
- [9] M. Coey, *Nature* **430**, 630 (2004).
- [10] M. Iizumi, T. F. Koetzle, G. Shirane, S. Chikazumi, M. Matsui, and S. Todo, *Acta Crystallogr. Sect. B Struct. Crystallogr. Cryst. Chem.* **38**, 2121 (1982).
- [11] E. J. W. VERWEY, *Nature* **144**, 327 (1939).
- [12] M. S. Senn, J. P. Wright, and J. P. Attfield, *Nature* **481**, 173 (2011).
- [13] J. P. Wright, J. P. Attfield, and P. G. Radaelli, *Phys. Rev. B* **66**, 214422 (2002).
- [14] D. I. Khomskii and M. V. Mostovoy, *J. Phys. A. Math. Gen.* **36**, 9197 (2003).
- [15] K. Kugel' and D. Khomskii, *Sov. J. Exp. Theor. Phys.* **37**, 725 (1973).
- [16] K. I. Kugel and D. I. Khomskii, *Sov. Phys. - Uspekhi* **25**, 621 (1982).
- [17] G. Subías, V. Cuartero, J. García, J. Herrero-Martin, J. Blasco, M. C. Snchez, and F. Yakhov, *J. Phys. Conf. Ser.* **190**, (2009).
- [18] J. Schlappa, C. Schüßler-Langeheine, C. F. Chang, H. Ott, A. Tanaka, Z. Hu, M. W. Haverkort, E. Schierle, E. Weschke, G. Kaindl, and L. H. Tjeng, *Phys. Rev. Lett.* **100**, 1 (2008).
- [19] D. J. Huang, H. J. Lin, J. Okamoto, K. S. Chao, H. T. Jeng, G. Y. Guo, C. H. Hsu, C. M. Huang, D. C. Ling, W. B. Wu, C. S. Yang, and C. T. Chen, *Phys. Rev. Lett.* **96**, 096401 (2006).
- [20] J. García and G. Subías, *J. Phys. Condens. Matter* **16**, R145 (2004).
- [21] M. Hepting Introduction: Transition Metal Oxides and Their Heterostructures. Springer Theses (Recognizing Outstanding Ph.D. Research). Spring, Cham (2017).
- [22] S. B. Wilkins, S. Di Matteo, T. A. W. Beale, Y. Joly, C. Mazzoli, P. D. Hatton, P. Bencok, F. Yakhov, and V. A. M. Brabers, *Phys. Rev. B - Condens. Matter Mater. Phys.* **79**, 2 (2009).
- [23] I. Leonov, A. N. Yaresko, V. N. Antonov, M. A. Korotin, and V. I. Anisimov, *Phys. Rev. Lett.* **93**, 146404 (2004).
- [24] J. Suntivich, W. T. Hong, Y. L. Lee, J. M. Rondinelli, W. Yang, J. B. Goodenough, B. Dabrowski, J. W. Freeland, and Y. Shao-Horn, *J. Phys. Chem. C* **118**, 1856 (2014).
- [25] H. Elnaggar, R. Wang, M. Ghiasi, M. Yañez, M. U. Delgado-Jaime, M. H. Hamed, A. Juhin, S. S. Dhesi, and F. De Groot, *Phys. Rev. Mater.* **4**, 024415 (2020).
- [26] R. Kukreja, N. Hua, J. Ruby, A. Barbour, W. Hu, C. Mazzoli, S. Wilkins, E. E. Fullerton,

- and O. G. Shpyrko, Phys. Rev. Lett. **121**, 177601 (2018).
- [27] W. Eerenstein, T. T. M. Palstra, T. Hibma, and S. Celotto, Phys. Rev. B **66**, 201101(R) (2002).
  - [28] See Supplemental Material at [for thin-film fabrication details, structural characterizations, and normalized two-time correlations for all temperatures.](#)
  - [29] Y. Tokura and N. Nagaosa, Science **288**, 5465 (2000).
  - [30] J. Chen, H-S. Hsu, Y-H. Huang, and D-J. Huang, Phys. Rev. B **98**, 085141 (2018).
  - [31] W.F.J. Fontijn, P.J. van der Zaag, M.A.C. Devillers, V.A.M Brabers, and R. Metselaar, Phys. Rev. B **56**, 5342 (1997).
  - [32] G. Perversi, E. Pachoud, J. Cumby, J. M. Hudspeth, J. P. Wright, S. A. J. Kimber, and J. Paul Attfield, Nat. Commun. **10**, 1 (2019).
  - [33] A. Bosak, D. Chernyshov, M. Hoesch, P. Piekarz, M. Le Tacon, M. Krisch, A. Kozłowski, A. M. Oles, and K. Parlinski, Phys. Rev. X **4**, 1 (2014).
  - [34] J. P. Hill, C. S. Nelson, M. V. Zimmermann, Y. J. Kim, D. Gibbs, D. Casa, B. Keimer, Y. Murakami, C. Venkataraman, T. Gog, Y. Tomioka, Y. Tokura, V. Kiryukhin, T. Y. Koo, and S. W. Cheong, Appl. Phys. A Mater. Sci. Process. **73**, 723 (2001).
  - [35] A. Nag, M. Zhu, M. Bejas, J. Li, H.C. Robarts, H. Yamase, A.N. Petsch, D. Song, H. Eisaki, A.C. Walters, M. García-Fernández, A. Greco, S. M. Hayden, and K-J Zhou, Phys. Rev. Lett., **125**, 257002 (2020).
  - [36] X.M. Chen, V. Thampy, C. Mazzoli, A.M. Barbour, H. Miao, G.D. Gu, Y. Cao, J.M. Tranquada, M.P.M. Dean, and S.B. Wilkins, Phys. Rev. Lett., **117**, 167001 (2016).
  - [37] V. Thampy, X.M. Chen, Y. Cao, C. Mazzoli, A.M. Barbour, W. Hu, H. Miao, G. Fabbri, R.D. Zhong, G.D. Gu, J.M. Tranquada, I.K. Robinson, S.B. Wilkins and M.P.M. Dean, Phys. Rev. B **95**, 241111(R) (2017).